Ali Y. Alharbi
Assistant Instructor,
Department of Mechanical Power and Refrigeration,
PAAET College of Technological Studies,
P.O. Box 42325,
Shuwaikh 70654, Kuwait
e-mail: aalharbi@paaetms.paaet.edu.kw

Deborah V. Pence[1]
Assistant Professor
e-mail: pence@engr.orst.edu

Rebecca N. Cullion
Research Assistant
e-mail: cullion@engr.orst.edu

Department of Mechanical Engineering,
Oregon State University,
204 Rogers Hall,
Corvallis, OR 97331-6001

Fluid Flow Through Microscale Fractal-Like Branching Channel Networks

Flow through fractal-like branching networks is investigated using a three-dimensional computational fluid dynamics approach. Results are used to assess the validity of, and provide insight for improving, assumptions imposed in a previously developed one-dimensional model. Assumptions in the one-dimensional model include (1) reinitiating boundary layers following each bifurcation, (2) constant thermophysical fluid properties, and (3) negligible minor losses at the bifurcations. No changes to the redevelopment of hydrodynamic boundary layers following a bifurcation are recommended. It is concluded that temperature varying fluid properties should be incorporated in the one-dimensional model to improve its predictive capabilities, especially at higher imposed heat fluxes. Finally, a local pressure recovery at each bifurcation results from an increase in flow area. Ultimately, this results in a lower total pressure drop and should be incorporated in the one-dimensional model. [DOI: 10.1115/1.1625684]

1 Introduction

Societal demands have resulted in extremely compact yet powerful electronic devices, which require high watt-density cooling techniques. Heat sinks incorporating microscale channels are very effective in this endeavor by increasing both the convective heat transfer coefficient as well as the convective surface area per unit volume in the heat sink.

However, the improved heat transfer provided by a series of parallel microchannels is not without drawbacks. The small diameter of the channels produces large pressure drops and nonuniform temperature distributions along the wall of the channel often occur. If used to cool an electronic component, a non-uniform temperature distribution, if significant enough, could result in uneven thermal expansion of the electronic device, possibly damaging it or affecting the electrical properties.

Tuckerman and Pease [1] first introduced the idea of microchannel heat sinks for cooling integrated circuits. Since that time, numerous investigations of single, straight microchannels and microchannel arrays in a heat sink have been conducted. Much of the experimental data prior to 2000, as noted in the review article by Sobhan and Garimella [2], are conflicting. Conclusions made by several of the original authors suggest that fluid and thermal transport phenomena through microchannels with characteristic flow diameters between 50 μm and 1 mm are different than macroscale phenomena. However, Obot [3] also reviewed numerous papers dealing with friction and heat and mass transfer in microchannels. Through careful reexamination of several works, he concluded that there is no supporting evidence to suggest that transport phenomena of liquids through microchannels is different from macrochannels. He further recommends use of conventional macroscale correlations for predicting pressure drop and heat transfer through such networks.

Bau [4] demonstrated, using a mathematical model, that a microchannel with a variable cross-sectional area can be optimized to reduce temperature gradients along the channel length. Reduction in the maximum heated surface temperature can be achieved by tapering a channel in the direction of the flow. However, a decrease in axial channel diameter can be accompanied by an increase in velocity and, hence, an increase in pumping power.

To improve the temperature uniformity while decreasing the pressure drop, Pence [5] proposed a fractal-like bifurcating flow network in a two-dimensional heat sink. The fractal-like flow network was designed using fixed diameter and length scale ratios between consecutive branching levels, as were proposed by West et al. [6] for natural transport systems. Using an optimization approach to minimize pumping power while adhering to a minimal volume constraint, Bejan [7] identified, on average, the same branching level ratios reported by West et al. [6]. The relation between engineered flow networks and those of natural systems is the subject of a book by Bejan [8].

Pence [9] developed a one-dimensional model, using macroscopic correlations, for predicting both the pressure distribution in, and wall surface temperature along, a fractal-like branching channel network. Results were compared to an array of straight channels having the same channel length and same convective surface area as the branching network. A lower maximum wall temperature along the fractal flow network was consistently noted for identical pressure drop, flow rate, and total pumping power through both flow networks. Chen and Chang [10], assuming fully developed conditions and negligible minor losses, assessed the pressure drop and heat transfer capacity of fractal-like channel networks for several levels of branching and various branching diameter ratios.

Wechsatol et al. [11] recently investigated, in a disk-shaped geometry similar to that proposed by Pence [5,9], the optimal channel length distribution, assuming fully developed, laminar flow with negligible minor losses. Length-scale ratios that vary at each bifurcating level were deemed optimal in terms of minimizing flow resistance.

2 Method of Analysis

Pence [5] developed a preliminary, non-optimized branching channel network in a disk-shaped heat sink using the following branching ratios:

$$\frac{d_{k+1}}{d_k} = n^{-1/3} \tag{1}$$

[1]To whom correspondence should be addressed.

Contributed by the Fluids Engineering Division for publication in the JOURNAL OF FLUIDS ENGINEERING. Manuscript received by the Fluids Engineering Division Jan. 22, 2003; revised manuscript received June 6, 2003. Associate Editor: K. D. Squires.

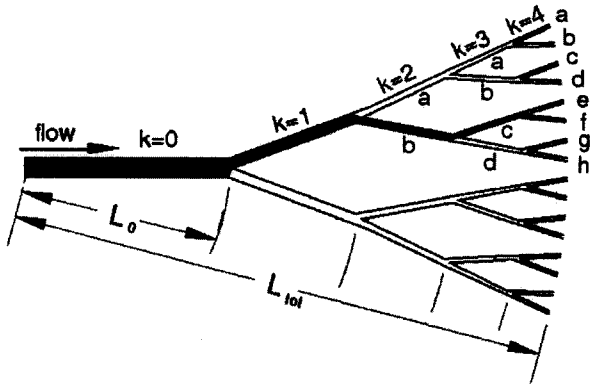

Fig. 1 Fractal-like branching channel network (shaded path includes branches $k=0$, $k=1$, $k=2b$, $k=3c$, $k=4f$)

$$\frac{L_{k+1}}{L_k} = n^{-1/2} \tag{2}$$

where d is the hydraulic diameter, L is the length of a channel segment, and n is the number of branches into which each channel splits. For the present analysis, $n=2$. Subscript k represents the lower-order branching level and subscript $k+1$ represents the higher-order branching level at a bifurcation. In reference to Fig. 1, the first branch emanating from the inlet flow plenum is the zeroth-order branch, i.e., $k=0$. The shaded region and the letters denoted in the figure are discussed later.

It is the objective of the present work to analyze the pressure distribution in microscale fractal-like branching channel networks using a three-dimensional computational fluid dynamics (CFD) analysis. The commercially available CFD package, STAR-CD, was employed. Results of these analyses are used to assess the validity of assumptions imposed in the one-dimensional model of Pence [9]. The initial flow network proposed by Pence [5] is employed for this purpose, as heat sinks with this flow network are available for experimental testing. Dimensions of the flow network are provided in Table 1. Note that the total channel length reported for the fractal-like flow network is the radial distance from the entrance of the $k=0$ branch to the exit of the $k=4$ branch level. The length of each branch is defined by radial distances in Fig. 1. Also note from Fig. 1 that the two new branches bifurcate asymmetrically from a lower level branch segment for $k \geqslant 1$.

2.1 One-Dimensional Predictive Model. In the one-dimensional model developed by Pence [9], the pressure distribution and wall temperature distribution along rectangular cross-section ducts in a fractal-like branching flow network are predicted using hydrodynamic theory and empirical correlations for heat transfer. The one-dimensional model is restricted to laminar flow with the assumptions that (1) both the thermal and hydrodynamic boundary layers redevelop following each channel bifurcation, (2) minor losses are negligible, and (3) thermophysical properties of the working fluid are held constant. It is the purpose of the present investigation to assess the validity of these three assumptions.

Table 1 Channel dimensions for fractal-like flow network ($\Sigma_{k=0}^{4} L_k = L_{tot} = 16.3$ mm)

k	H_k (mm)	w_k (mm)	d_k (mm)	L_k (mm)	α_k
0	0.250	0.539	0.342	5.80	0.389
1	0.250	0.296	0.271	4.10	0.750
2	0.250	0.189	0.215	2.90	0.830
3	0.250	0.130	0.171	2.05	0.562
4	0.250	0.093	0.136	1.45	0.400

The pressure drop correlation in White [12], which includes increased pressure due to developing flow conditions, and the Nusselt number data for simultaneously developing thermal and hydrodynamic boundary layers from Wibulswas [13], and referred to in Shah and London [14], are employed in the one-dimensional model. Water is used as the working fluid, and a constant heat flux is applied to the walls of the ducts composing the flow network.

2.2 Three-Dimensional Computational Model. Numerical simulations were performed using the finite-volume based, commercially available computational fluid dynamics (CFD) software STAR-CD (version 3.0B) from Computational Dynamics Limited. Three-dimensional CFD simulations were performed with water as the working fluid for a fractal-like flow network and a parallel flow network. Held identical between these flow networks are the total channel length, the terminal branch hydraulic diameter, the convective surface area, the heat flux applied to the convective surface area, and the total pumping power. Note that a representative path length for the fractal network is shown as a shaded region in Fig. 1. The steady, incompressible form of the three-dimensional continuity, momentum and energy equations governing the transport in this investigation are as follows:

Continuity:

$$\frac{\partial V_i}{\partial x_i} = 0 \tag{3}$$

Momentum:

$$\rho\left(\frac{\partial (V_i V_j)}{\partial x_i}\right) = \frac{\partial}{\partial x_i}\left(\mu \frac{\partial V_j}{\partial x_i}\right) - \frac{\partial p}{\partial x_i} \tag{4}$$

Energy Equation:

$$\rho\left(\frac{\partial (V_i c_p T)}{\partial x_i}\right) = \frac{\partial}{\partial x_i}\left(\lambda \frac{\partial T}{\partial x_i}\right) \tag{5}$$

Consistent boundary conditions between the two flow networks are the inlet and exit flow boundary conditions and no slip, impermeable conditions at all walls. At the inlet, the bulk fluid temperature is fixed, as is the velocity profile, which is assumed uniform. The flow discharges to a water-filled reservoir assumed to be at atmospheric pressure at the point of discharge. A uniform heat flux is applied at the wall of the flow network.

The steady, incompressible, three-dimensional continuity, energy and momentum equations are solved using a central differencing scheme for the diffusion terms and the STAR-CD MARS scheme for the advection terms. MARS stands for monotone advection and reconstruction scheme. It is a two-step scheme of second-order accuracy which, of the available discretization schemes, is least sensitive to errors resulting from mesh structure and skewness. Pressure-velocity coupling was accomplished using the SIMPLE method. Under-relaxation parameters of 0.2, 0.7, and 0.95 were employed for pressure, velocity, and temperature, respectively, in this study.

3 Results and Discussion

Three-dimensional computational results are sought that provide a means for assessing the assumptions imposed in the one-dimensional model by Pence [9] for predicting pressure distributions through fractal-like flow networks. Again, these assumptions include (1) reinitiation of hydrodynamic and thermal boundary layers following each channel bifurcation, (2) negligible minor losses, and (3) constant thermophysical properties of the working fluid.

Of particular interest from the three-dimensional investigation is the axial pressure distribution. Fluid properties of the water are held constant initially, and then allowed to vary with temperature.

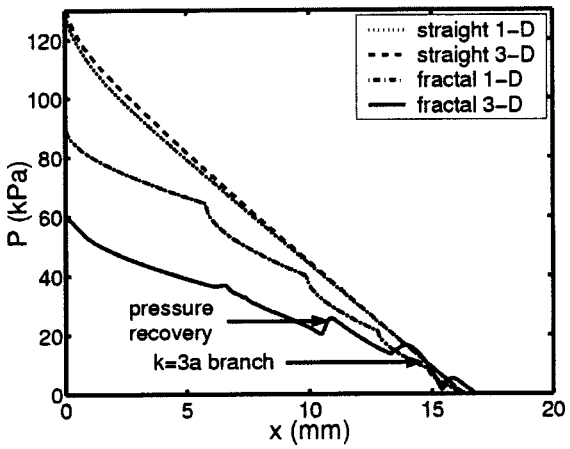

Fig. 2 Constant property pressure distribution through fractal-like and straight channel networks

The three-dimensional model results assuming constant properties are compared to the one-dimensional model results to assess the validity of assumptions 1 and 2. To assess the validity of assumption 3, results from the three-dimensional model with fluid properties allowed to vary with temperature are compared to three-dimensional results assuming constant thermophysical properties.

The three-dimensional CFD simulated pressure distribution along a fractal-like network is also compared to that through a single straight channel. The straight channel exists within a series of parallel channels having an identical hydraulic diameter as the terminal channel in the fractal-like flow network. Also identical between the fractal-like and straight channel networks are channel length, convective surface area, heat flux, and pumping power. Three-dimensional simulated pressure drop through a fractal-like network with an inlet flow plenum is compared with that obtained experimentally. In previous investigations, Pence [5,9] provided one-dimensional comparisons of fractal-like heat sinks to parallel channel heat sinks with different heat sink surface areas, with differing total channel lengths, and under various flow rate conditions.

3.1 Constant Property Analysis. As was done in Pence [9], results through a fractal-like flow network are compared to a network of parallel, straight channels with the same hydraulic diameter as the terminal branch of the fractal channel network, 136 μm, but with a square cross-section. The radial distance from the edge of the inlet plenum to the exit plenum is 16.3 mm and assumed to be the total length, regardless of path taken, through a fractal network. The total channel length and the convective wall surface area for the straight channel network are the same as for the fractal-like network. Two fractal-like and thirteen parallel flow networks are investigated, yielding total convective surface areas, defined by the walls of the flow networks, of 115 mm^2 and 114 mm^2, respectively.

To achieve identical pumping power between the straight and fractal-like flow networks, the total fluid flow through the thirteen straight channels is 1.2 ml/s and 1.8 ml/s through the two fractal-like flow networks. These flow rates ensure laminar flow through each channel in each flow network, with the largest Reynolds number, on the order of 2000, occurring in the largest diameter branch of the fractal network. A constant heat flux of 45 W/cm^2 is applied to the periphery of each channel in both networks. Properties of the coolant fluid are held constant in this part of the analysis, and are assessed at the average temperature of the inlet and exit bulk fluid temperatures.

Centerline pressure distributions for both flow networks are shown in Fig. 2. The pressure distribution presented from the three-dimensional model simulation is that along the path defined in Fig. 1 by the following branches: $k=0$, $k=1$, $k=2a$, $k=3a$, and $k=4a$. Note that each branching level is identified by a number, i.e., $k=0$ is the original branch, and each branch segment of each level beyond $k=1$ is identified by the branch level as well as by a letter, *a*, *b*, *c*, etc. Due to asymmetry in the fractal-like flow network shown in Fig. 1, the three-dimensional pressure distribution might be slightly different from path to path. Based on the three-dimensional CFD simulations, the pressure drop through the straight channel network is about 70 kPa higher than that through the fractal-like network. The one-dimensional model and the three-dimensional CFD results for the straight channel are within 4%, suggesting that the one-dimensional model provides very good predictions for flow through a straight, constant hydraulic diameter microscale channel. However, for the fractal-like network, the one-dimensional model over-predicts the pressure drop by nearly 50%. Note that the total length of the fractal network in the three-dimensional CFD model, which was designed by dividing 16.3 mm into radial lengths adhering to Eq. (2), is slightly longer than the path length in the one-dimensional model.

Three possible reasons why the one-dimensional model over-predicts the three-dimensional simulations are considered. First, for the fractal-like network in the one-dimensional model, the velocity profile was assumed uniform at the inlet of each successive branching channel, resulting in the redevelopment of the hydrodynamic boundary layer at the entrance of each fractal segment. This is assumed at each wall, even though it is not truly anticipated at the top or bottom channel walls between branching levels due to a constant channel depth. Hence, it is anticipated that this may result in a greater pressure drop predicted from the one-dimensional model. Despite the difference in total pressure drop predicted from the one-dimensional model and the three-dimensional CFD model, the distributions follow a similar trend in the developing flow region, suggesting that the assumption of hydrodynamic boundary layer redevelopment at every wall following a bifurcation should be retained.

Second, noted in the three-dimensional pressure distribution is an instantaneous pressure recovery at each bifurcation, which tends to lower the total pressure drop. A pressure recovery is absent from the one-dimensional distribution. The observed pressure recovery in the three-dimensional simulations may result from the tapered increase in cross-sectional area, which acts similarly to a 'diffuser' following each bifurcation. Note that the pressure recovery is largest for the higher order branches, which have smaller branching angles. In the direction of increasing branching level, branching angles are 40, 36, 29, and 22 deg, respectively. The magnitude of the pressure recovery also depends upon the flow path taken due to the asymmetry of each bifurcation.

Third, an additional trend not noticed in the one-dimensional model is the three-dimensional pressure distribution through the $k=3a$ branch. The distribution in this branch is similar to that through the $k=3d$ branch, but qualitatively different from all other branch distributions. To explain the observed pressure recovery and the anomalous $k=3a$ pressure distribution, details of the flow characteristics are further investigated.

Details of the flow field just upstream and immediately following each bifurcation are investigated to gain better insight into the flow phenomena responsible for the observed pressure recovery. The flow path investigated is that shaded in Fig. 1. Because the axial flow direction changes through each branch, a separate coordinate system is established for each branch segment in each level. The origin of the coordinate system is the apex of the inner wall, as noted in Fig. 3. Variable *x* represents the axial flow direction, *y* represents the spanwise direction from the origin at the inner wall to the outer wall, and *z* is measured from the bottom of the channel to the top of the channel. Because *z* is always measured from the bottom of the channel, the right-hand rule is violated for the following branches: $k=2b$, $k=3b$, $k=3d$, $k=4b$, $k=4d$, $k=4f$, and $k=4h$. It is also relevant to note that the beginning of the outer wall of the $k=3c$ branch is not aligned

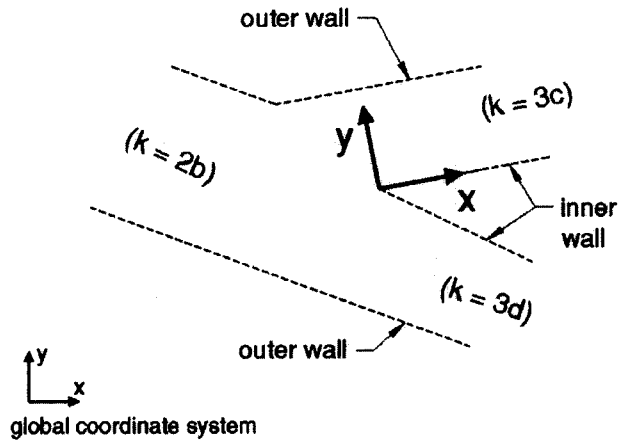

Fig. 3 Local coordinate system for $k=3c$ branch. Note that z is always out of the page and that the channel $k=3d$ is tapered.

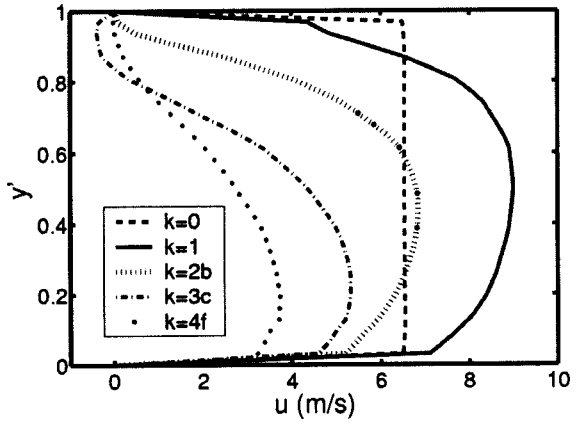

Fig. 5 Axial velocity profiles at $x'=0$ and $z'=0.5$ for all branches along shaded path in Fig. 1

with the origin, but rather corresponds to a negative value of x relative to the local coordinated system shown in Fig. 3.

In Fig. 4 are shown three-dimensional velocity magnitude contours at mid-depth in the x-y plane ($z'=0.5$) between the $k=0$ and $k=1$ branches. Note that $z'=z/H$, where H is the depth of the channel and equal to 250 μm. As the cross-sectional flow area is increased following the bifurcation, the total volume flow is decelerated. This is most noticeable along the outer channel walls. It is also clear from Fig. 4 that the boundary layer at the outer wall does not reinitiate as is assumed in the one-dimensional model. However, development of a new laminar boundary layer is clearly noted at the inner wall with a pronounced influence of the inner wall felt upstream. The two first-level branches ($k=1$) have mirrored image profiles due to symmetry in the angle at which they bifurcate from the $k=0$ branch.

In Fig. 5, axial (x-component) velocity profiles at the inlet, $x'=0$, of each branch taken at the x-y midplane, $z'=0.5$, along the shaded path in Fig. 1 are provided. Data are normalized by the width, w, of each branching level, i.e., $y'=y/w$, which decreases for increasing values of k. Values of y' equal to 0 and 1, respectively, represent the inner and outer walls, while values of z' equal to 0 and 1, respectively, represent the bottom and top walls of the channel network. The variable x' represents the axial distance along the inner wall normalized by the inner wall length. Of particular interest in Fig. 5 are (1) the reduction in maximum velocity with each branching level, which is anticipated due to the increase in total flow area following each bifurcation, (2) the initiation of a boundary layer at the inner wall which originates following a bifurcation, (3) the asymmetry in the velocity profiles due to asymmetry in the bifurcating angle, and (4) the flow reversal near the outer wall observed for the $k=3c$ branch.

Shown in Fig. 6 are the axial velocity profiles at the inlet, $x'=0$, of each branching level along the shaded path in Fig. 1, taken from the x-z midplane at $y'=0.5$. Unlike the velocity profiles in Fig. 5, which are asymmetric due to asymmetric branching angles, the velocity profiles in Fig. 6 are symmetric. This is attributed to a constant channel depth. Note the absence of a redeveloping boundary layer at the top and bottom walls.

In Fig. 7 and Fig. 8 are plotted the axial velocity profiles at the exit of each channel along the flow path shaded in Fig. 1. Figure 7 shows the axial velocity profiles at $x'=1$ for the x-y midplane ($z'=0.5$), whereas Fig. 8 shows the axial velocity profiles at $x'=1$ for the x-z midplane ($y'=0.5$). In comparing the profiles in Fig. 7 with those in Fig. 5, the development of boundary layers from channel inlet to exit at the inner wall ($y'=0$) for the $k=2b$ and $k=3c$ branches is evident. The profile for the $k=1$ branch in Fig. 7 shows an accelerating flow near the inner wall at the channel exit, but shows clearly the boundary layer development at the outer wall ($y'=1$). The $k=0$ branch in Fig. 7 shows a symmetric profile with flow deceleration near the centerline. The $k=4f$ branch, which discharges to the exit plenum, is also sym-

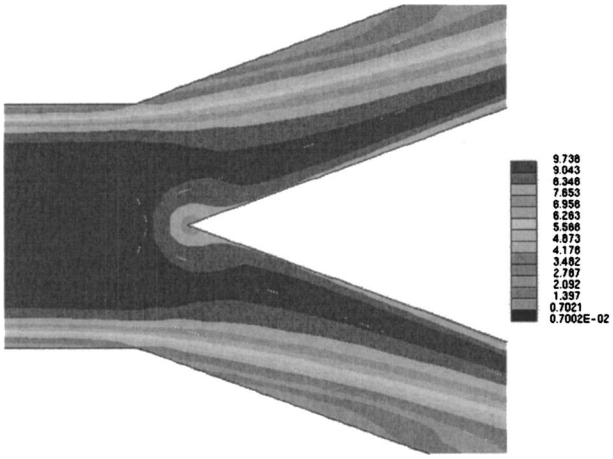

Fig. 4 Mid-depth, $z'=0.5$, velocity magnitudes at the junction between branching level 0 and level 1

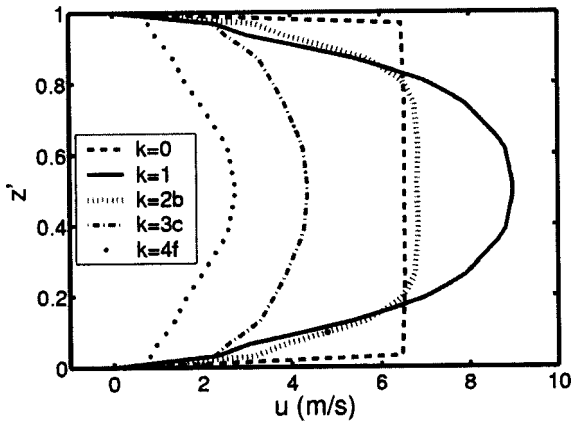

Fig. 6 Axial velocity profiles at $x'=0$ and $y'=0.5$ for all branches along shaded path in Fig. 1

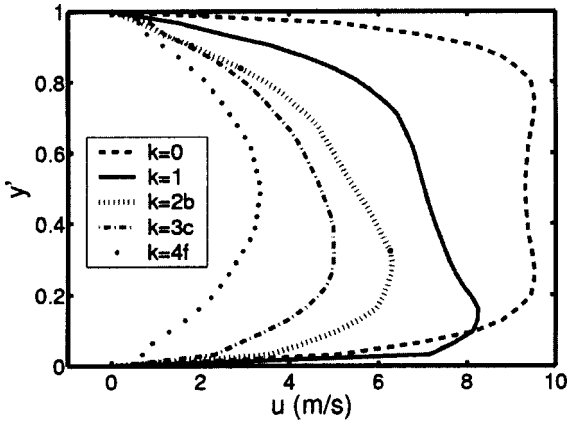

Fig. 7 Axial velocity profiles at $x'=1$ and $z'=0.5$ for all branches along shaded path in Fig. 1

metric. The $k=3c$ profile in Fig. 7 shows that the negative flow near the outer wall at the branch inlet, shown in Fig. 5, is positive at the branch exit.

Figure 8 shows the x-z midplane ($y'=0.5$) axial velocity profiles at the exit, $x'=1$, of each branch in the path in Fig. 1. Notice that the $k=0$ branch, the only branch which symmetrically bifurcates, and the $k=4f$ branch which discharges into the plenum, do not exhibit flow deceleration at the centerline. However, the branches anticipating an asymmetric bifurcation show noticeable deceleration at the centerline in the $y'=0.5$ midplane. The shape of the decelerated profiles in Fig. 8 and the asymmetric profiles in Fig. 7 may be a consequence of a secondary flow.

Figures 9 and 10 show the y-z component velocity vectors at $x'=1$ for branch $k=0$ and $k=1$, respectively. The largest magnitude of the nonaxial flow vectors in Fig. 9 is 1.2 m/s, approximately 10% of the axial velocity at the centerline. This secondary flow is symmetric about both the $y'=0.5$ and $z'=0.5$ axes, in agreement with the symmetric bifurcation following the exit of this channel. The regions along $z'=0.5$ in Fig. 9 where the secondary flow magnitude, denoted by the length of the velocity vector arrows, is highest coincide with the maximum velocity locations observed in Fig. 7 for the $k=0$ branch.

Figure 10 shows the y-z component velocity vectors at the exit of the $k=1$ branch. The largest magnitude of the non-axial flow vectors is 2 m/s, approximately 20% of the axial velocity at the centerline. There is an asymmetry noted in this figure, which shows a strong secondary flow toward branch level $k=2b$ (the

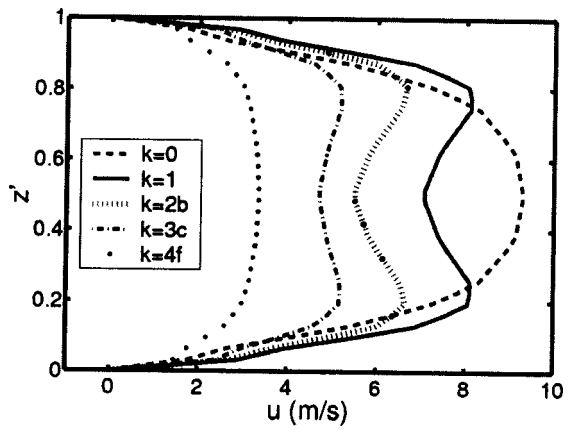

Fig. 8 Axial velocity profiles at $x'=1$ and $y'=0.5$ for all branches along shaded path in Fig. 1

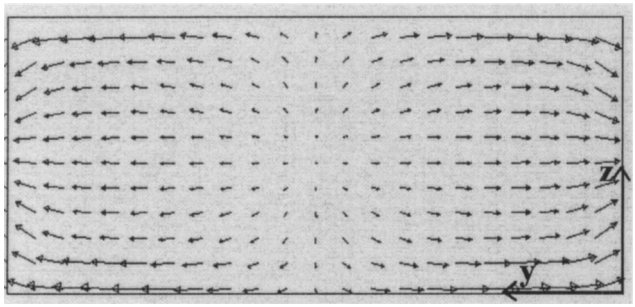

Fig. 9 Nonaxial velocity vectors at $x'=1$ for branch $k=0$

right hand side of the figure). The flow toward branch $k=2a$ (the left hand side of the figure) appears to be primarily in the axial direction, with little secondary flow. Again, the secondary flow along $z'=0.5$ is strongest nearer $y'=0$, in agreement with the largest axial flow observed for branch $k=1$ in Fig. 7. The velocity profiles in Figs. 7 and 8 demonstrate a tendency for flow diverted or accelerated in one direction, i.e., in the x-y plane, to decelerate flow in the orthogonal direction, i.e., the x-z plane.

Figure 11 shows how a particle with no mass, placed in the flow field near $y'=0.9$ and $z'=0.65$ near the inlet to branch segment $k=3d$, follows a circulatory flow pattern. The particle trace in Fig. 11, shown from an x-y projection, is actually three-dimensional in nature and is a consequence of a strong secondary flow. In summary, it appears that flow deceleration and recirculation resulting from an increase in flow area and a distinct bifurcation angle may be responsible for the pressure recovery observed

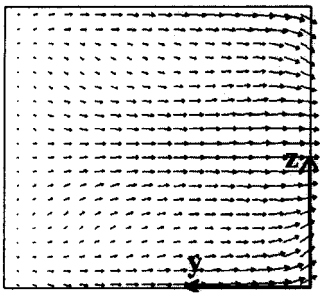

Fig. 10 Nonaxial velocity vectors at $x'=1$ for branch $k=1$

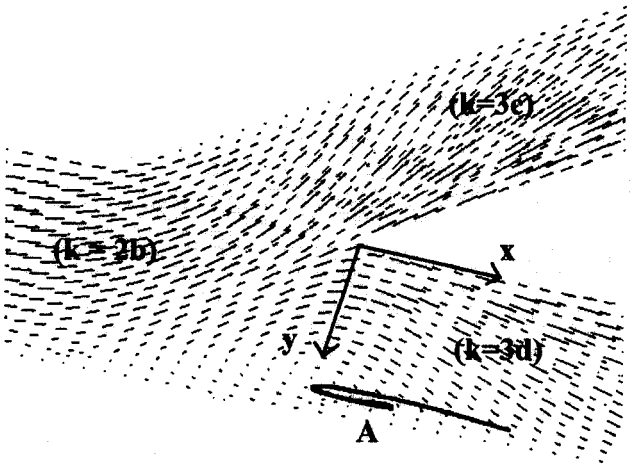

Fig. 11 Particle trace of massless particle introduced near $(x',y',z')=(0,0.9,0.65)$ of $k=3d$ branch

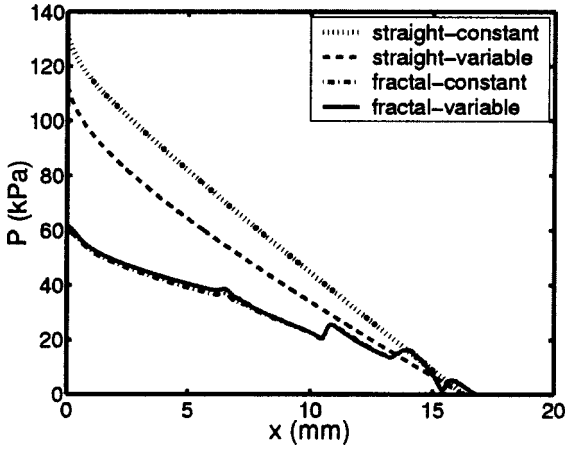

Fig. 12 Three-dimensional CFD pressure distributions for fractal-like and straight channel networks with constant and variable fluid properties

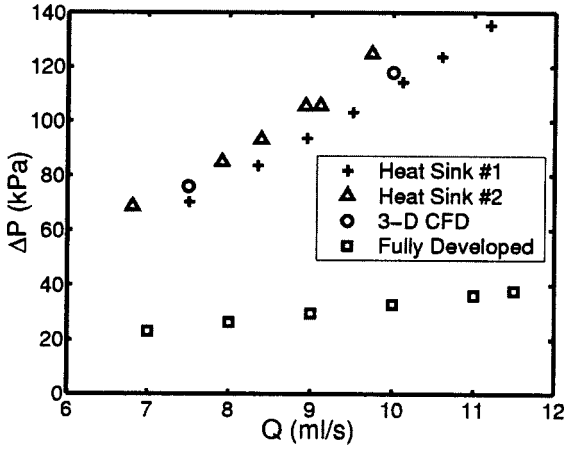

Fig. 13 Experimental pressure drop from two prototypes compared with pressure drop from three-dimensional CFD model with an inlet plenum. Fully developed assessments are based on theory with no inlet plenum.

at each bifurcation in Fig. 2. The degree of recirculation appears to be heavily dependent on the angle at which bifurcation occurs.

Finally, recall that the pressure distribution through the $k=3a$ branch in Fig. 2 is qualitatively different than that through all other branches, except for the $k=3d$ branch. Because all four $k=3$ branches exhibit a negative flow near the outer wall at $x'=0$, but only $k=3a$ and $k=3d$ branches are tapered, the shape of the pressure distribution through the $k=3a$ branch in Fig. 2 is attributed to the tapered channel geometry.

In summary, the general shapes of the one-dimensional and three-dimensional pressure distributions simulated assuming constant properties are qualitatively similar, with the exception of the pressure recovery and the distribution through the tapered channel. For this reason, incorporation of minor losses, or more appropriately the increased area, at the bifurcations in the one-dimensional model appears necessary. It also appears that the assumption of a redeveloping hydrodynamic boundary layer at all walls, although it is physically only occurring at the inner walls, provides a good prediction of the pressure distribution in the entrance region of each branch. Further assessment of this assumption can be made once minor losses due to the bifurcation are incorporated.

3.2 Variable Property Analysis. Specific heat, thermal conductivity and molecular viscosity of water change by 1.6%, 20% and 84%, respectively, over the range of temperatures from 20°C to 100°C. Although the temperature dependence of specific heat can be neglected, it appears the same is not so for thermal conductivity and viscosity. In this section, the validity of assuming constant properties in the one-dimensional model is investigated. Results from the three-dimensional CFD model run with constant, and then run with temperature-dependent thermophysical properties are compared. Thermal conductivity and molecular viscosity are determined, for the constant temperature case, using the average temperature between the inlet and exit bulk fluid temperatures.

Figure 12 shows the three-dimensional CFD pressure distributions in the straight channel network and the fractal-like branching channel network with temperature-dependent properties and with constant, fluid properties. The pressure distribution in the fractal-like network is along the path defined by the following branches in Fig. 1: $k=0$, $k=1$, $k=2a$, $k=3a$, and $k=4a$. The total pressure drop simulated using constant fluid properties for the straight channel network is noticeably higher, approximately 17%, than for temperature dependent fluid properties. In contrast, for the fractal-like flow network the variable property effects are negligible. The reason for this is that the straight channel case has a higher velocity for the same power input; therefore, the shear stress for the straight channel is much higher than that through the fractal-like flow network. Hence, the viscosity has a more significant influence on the pressure drop through the straight channel array.

For water, molecular viscosity decreases with increases in temperature. For a fixed mass flow rate, the decreased viscosity results in a reduced wall stress; hence, a lower pressure drop. On the other hand, the Reynolds number, by definition, tends to increase with a decrease in molecular viscosity. The increased Reynolds number would tend to contribute to an increase in the hydraulic entrance length, which would in turn result in an increase in pressure drop. Therefore, of these two competing factors, the lower shear stress has a more significant effect on the pressure drop. The differences in pressure drop between the constant and variable fluid properties cases suggest that the one-dimensional model should be modified to account for temperature dependent fluid properties in order to be a more dependable predictive tool. This will be of more importance at higher heat fluxes.

3.3 Numerical Uncertainty. Numerical errors reported from the three-dimensional CFD analysis include those caused by mesh spacing, irregularity and nonorthogonality, and the choice of the differencing scheme used for the convective term. These are typically less than 0.1% and 0.2%, respectively, for pressure in the straight channel and fractal-like channel networks, with localized errors on the order of $\pm 0.5\%$ and $\pm 1.5\%$. Anticipated errors in the one-dimensional model include discretization errors that, based on a spatial grid twice the resolution as that employed, are computed to be less than 0.1 Pa. Both three-dimensional CFD and one-dimensional model results exhibit errors due to imposed assumptions, which are expected to be large when fluid properties are held constant and when minor losses in the one-dimensional model for the fractal flow network are neglected.

3.4 Experimental Analysis. Doerr [15] provided pressure drop data for two prototypes of the fractal-like heat sink. Because the experimental test devices had an inlet plenum, this plenum was modeled in a three-dimensional CFD analysis assuming a uniform inlet velocity to the plenum. Fluid properties were assumed constant in the CFD analysis because all experiments were conducted with water at atmospheric conditions. Pressure drop through both heat sink test fixtures for several flow rates are provided in Fig. 13. Three-dimensional CFD simulated pressure drop for two flow rates within the flow rate range of experimental data are also shown in Fig. 13. Pressure drop through a fractal flow network was also estimated as a function of flow rate assuming no

inlet plenum and fully developed flow conditions. These results are added to Fig. 13 as a means to assess the anticipated error in pressure drop due to assuming negligible losses through the plenum and at the bifurcations, and by assuming fully developed flow conditions.

Experimental errors in pressure drop and flow rate are on the order of ± 3 kPa and ± 0.05 ml/s, respectively, as determined from the standard error of the fit to calibration data and the accuracy of the standards employed in the calibration process. Calibration standards were dead weight testers for the pressure transducers and a catch-and-weigh method for the flowmeters. The aforementioned errors do not take into account uncertainties in wall surface characteristics or actual channel dimensions following the bonding process. Based on a sensitivity analysis using measured discrepancies in channel dimensions, these are anticipated to result in another $\pm 15\%$ uncertainty in the experimental pressure drop. Figure 13 suggests that the three-dimensional CFD is adequately validated by experiments for flow with an inlet plenum. Because flow without an inlet plenum cannot be tested experimentally, experimental validation of CFD pressure results is assumed by extrapolation.

4 Conclusions and Recommendations

In the present research, flow through straight and fractal-like branching networks was investigated using a three-dimensional CFD approach. Results of the pressure distribution through a three-dimensional flow network were compared to that predicted using a one-dimensional model. The one-dimensional model incorporates macroscale correlations. A three-dimensional model was used to assess the validity of, and provide insight for improving, assumptions imposed in the one-dimensional model. Assumptions include (1) redeveloping flow conditions following each bifurcation, (2) negligible minor losses, and (3) constant thermophysical fluid properties.

Pressure distributions for a straight channel network and for a fractal-like branching channel network assuming both constant and temperature dependent fluid properties were considered. Constant between the two configurations are length of a single flow path from inlet to exit, the convective surface area, the terminal hydraulic diameter, the applied heat flux and the supplied pumping power required to move the fluid through the flow network.

The three-dimensional CFD results show that the pressure drop through the fractal-like network is 50% less than that through the straight channel network. Results from the one-dimensional and three-dimensional models, both assuming constant properties, are compared to assess the validity of the developing flow and negligible minor losses assumptions. Although the one-dimensional model well predicts, within 4%, the three-dimensional CFD pressure drop for a straight channel network, a noticeable difference in pressure drop, approximately 30%, for the fractal-like network was observed between the two models. This difference in pressure drop is primarily the result of a local pressure recovery at each bifurcation. Axial velocity profiles along the flow network demonstrate asymmetric flow development as well as a region of negative flow. Nonaxial velocity vectors in the cross-section plane at a channel exit, immediately preceding a bifurcation, show a strong secondary flow. The pressure recovery is believed to be a consequence of these secondary flow conditions resulting from an increased cross-sectional flow area and the presence of a bifurcating channel.

Comparison of the three-dimensional CFD pressure drop for both networks with and without variable fluid properties provides a means of assessing the assumption of constant thermophysical properties. Pressure drop results are slightly higher with constant properties versus variable properties, on the order of 17% for the straight channel design. This was attributed to the decrease in wall shear stress resulting from a decrease in viscosity with an increase in fluid temperature. Finally, a three-dimensional CFD model with an inlet plenum and assuming constant properties was validated with experimental data from two prototypes.

It is concluded that temperature varying fluid properties and minor loss effects following a bifurcation should be incorporated in the one-dimensional model to improve its predictive capabilities. Assuming redevelopment of the hydrodynamic boundary layer following each bifurcation seems to provide plausible trends in the pressure distribution near the inlet of each channel branch.

Nomenclature

H = channel height, mm
L = channel length, mm
T = temperature, K
V = total velocity, m/s
c_p = specific heat, J/kg K
d = hydraulic diameter, mm
k = branch level
n = number of bifurcating channels per segment
p = pressure, Pa
u = axial velocity component, m/s
w = channel width, mm
x = axial direction
y = spanwise direction
z = transverse direction
x' = dimensionless axial direction (x/L)
y' = dimensionless spanwise direction (y/w)
z' = dimensionless transverse direction (z/H)
α = aspect ratio $(\min[w,H]/\max[w,H])$
λ = thermal conductivity, W/m K
μ = molecular viscosity, N s/m^2
ρ = density, kg/m^3

Subscripts

i, j = coordinate indices

References

[1] Tuckerman, D. B., and Pease, R. F. W., 1981, "High-Performance Heat Sinking for VLSI," IEEE Electron Device Lett., **EDl-2**(5), pp. 126–277.
[2] Sohban, B. S., and Garimella, S. V., 2001, "A Comparative Analysis of Studies on Heat Transfer and Fluid Flow in Microchannels," Microscale Thermophys. Eng., **5**, pp. 293–311.
[3] Obot, N. T., 2000, "Toward a Better Understanding of Friction and Heat/Mass Transfer in Microchannels—A Literature Review," *Proc. International Conference on Heat Transfer and Transport Phenomena in Microscale*, Banff, Canada, Begell House, New York, pp. 72–79.
[4] Bau, H. H., 1998, "Optimization of Conduits' Shape in Micro Heat Exchangers," Int. J. Heat Mass Transfer, **41**, pp. 2717–2723.
[5] Pence, D. V., 2000, "Improved Thermal Efficiency and Temperature Uniformity Using Fractal-Like Branching Channel Networks," *Proc. International Conference on Heat Transfer and Transport Phenomena in Microscale*, Banff, Canada, Begell House, New York, pp. 142–148.
[6] West, G. B., Brown, J. H., and Enquist, B. J., 1997, "A General Model for the Origin of Allometric Scaling Laws in Biology," Science, **276**, pp. 122–126.
[7] Bejan, A., 1997, "Constructal Tree Network for Fluid Flow Between a Finite-Size Volume and One Source or Sink," Rev. Gen. Therm., **36**, pp. 592–604.
[8] Bejan, A., 2000, *Shape and Structure, from Engineering to Nature*, Cambridge University Press, Cambridge, UK.
[9] Pence, D. V., 2002, "Reduced Pumping Power and Wall Temperature in Microchannel Heat Sinks With Fractal-Like Branching Channel Networks," Microscale Thermophys. Eng., **6**(4), pp. 319–330.
[10] Chen, Y., and Cheng, P., 2002, "Heat Transfer and Pressure Drop in Fractal Tree-Like Microchannel Nets," Int. J. Heat Mass Transfer, **45**, pp. 2643–2648.
[11] Wechsatol, W., Lorente, S., and Bejan, A., 2002, "Optimal Tree-Shaped Networks for Fluid Flow in a Disc-Shaped Body," Int. J. Heat Mass Transfer, **45**, pp. 4911–4294.
[12] White, F. M., 1991, *Viscous Fluid Flow*, McGraw-Hill, New York.
[13] Wibulswas, P., 1966, "Laminar Flow Heat Transfer in Non-Circular Ducts," Ph.D. dissertation, University of London, London, UK.
[14] Shah, R. K., and London, A. L., 1978, "Laminar Flow Forced Convection in Ducts," *Advances in Heat Transfer*, Supplement 1, Academic Press, New York.
[15] Doerr, A., 2000, "Bifurcating Fractal Microchannel Heat Exchanger," Senior Project Report, Oregon State University, Corvallis, OR.